Materials Science for Energy Technologies 6 (2023) 89–93

Contents lists available at ScienceDirect

Materials Science for Energy Technologies

journal homepage: www.keaipublishing.com/en/journals/materials-science-for-energy-technologies

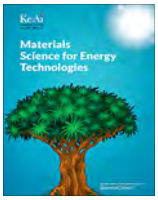

Manufacture and characterization of indicator electrodes from PPy + H_2SO_4 and PPy + Sulfonic acid as a urea sensor using urease enzyme immobilization technique in PVA

S. Abd Hakim [a,*], Martha Rianna [b], Abdul Rais [a]

[a] Physics Department, Faculty of Mathematics and Natural Sciences, Universitas Negeri Medan, Medan, Indonesia
[b] Universitas Sumatera Utara, Medan, 20155, Indonesia

ARTICLE INFO

Article history:
Received 23 November 2022
Accepted 24 November 2022
Available online 29 November 2022

Keywords:
PVA-enzyme/GA-2.9%/PPy+H2SO4 or sulphonic acid/PVC-KTpClPB-o-NPOE
Biosensor potentiometry
Immobilization of urease enzyme

ABSTRACT

Research has been carried out on indicator electrodes (1) PVA-Enzyme/PVC-KTpClPB, sensitivity 19,069 mV/decade, detection range 1.10^{-5}–5.10^{-4} M, detection limit 1.10–5 M. The width of the peak UV–vis absorbance is narrow (2) PVA-Enzyme/GA-2.9 %/PVC-KTpClPB wide UV–vis absorbance peak but the absorbance peak decreased, (3) PVA-Enzyme/GA-2.9 %/PVC-KTpClPB-o-NPOE XRD analysis amorphous spectral pattern appeared (4) PVA-Enzyme/GA-2.9 %/PPy + H_2SO_4/PVC-KTpClPB-o-NPOE (5) PVA-Enzyme/GA-2.9 %/PPy + Sulfonic Acid/PVC-KTpClPB-o-NPOE, amorphous spectrum pattern in (4) and (5) were greatly reduced for the enzyme variation of 0.6 g in 0.5 mL (50 % water + 50 % alcohol). GA plays a role in increasing the detection range, o-NPOE forms amorphous, enzyme variations increase the intensity of the XRD spectrum pattern. The method of developing a gradual modification of the indicator electrode membrane by cross-linking GA, o-NPOE, conductive polymer. The best results were obtained at the indicator electrode PVA-Enzyme/GA-2.9 %/PPy + Sulfonic Acid/PVC-KTpClPB-o-NPOE. Analysis of the linear curve of the sample EI_5-1 with a sensitivity of 41.56 mV/decade, a detection range of 10^{-4}–10^{-1} M and a detection limit of 10^{-4} M, R^2 = 97.51 %. The best indicator electrode is EI_5-1.

1. Introduction

Modification of the indicator electrode membrane layer started from (1) PVA-Enzyme/PVC-KTpClPB [1,2] PVA-Enzyme/GA-2.9 %/PVC-KTpClPB [1–3] PVA-Enzyme/GA-2.9 %/PVC-KTpClPB-o-NPOE, [4] PVA-Enzyme/GA-2.9 %/PPy + H_2SO_4/PVC – KTpClPB-o-NPOE, PVA-Enzyme/GA-2.9 %/PPy + Sulfonic Acid/PVC-KTpClPB-o-NPOE.

Each indicator electrode is given the notation EI_1, EI_2, EI_3, EI_4 and EI_5. EI_1 narrow absorbance spectrum pattern resulting in a small detection range modified to EI_2. EI_2 was modified by adding a GA layer at variations of 2.6 %, 2.9 % and 3.0 % in PVA-Enzyme from EI1. The GA solution was analyzed by UV–vis. The absorbance spectrum pattern increases the width of the absorption peak which affects the detection range (see Fig. 1a). EI_2 modification was continued by adding o-NPOE solution at variations of 61 % and 66 % in PVC-KTpClPB solution. The PVC-KTpClPB-o-NPOE solution was analyzed by UV–vis to produce the absorbance spectrum pattern seen in Fig. 1b. EI_2 analysis with XRD produces an amorphous spectral diffraction pattern around the 2theta angle of 20–25 degrees accompanied by a decrease in energy intensity, see Fig. 2a. The formation of an amorphous spectrum pattern and a decrease in intensity.

Based on Figs. 1 and 2, the researchers continued to modify the indicator electrode membrane with a conducting polymer material, namely PPy. This PPy can only dissolve in H2SO4 and Sulphonic Acid. H_2SO_4 is soluble at a concentration of 8 M while sulfonic acid is soluble at a concentration of 1 M. Modification of the electrode membrane in sequence (1) PVA-Enzyme/GA-2.9 %/PPy + H_2SO_4/PVC-KTpClPB-o-NPOE, denoted EI_4-1 (2) PVA-Enzyme/GA-2.9 %/PPy + Sulfonic Acid/PVC-KTpClPB-o-NPOE denoted EI_5-1. Modification procedures EI_4-1 and EI_5-1, variations in the number of drops of urease enzyme are one drop and three drops, the results of the analysis can be seen in Fig. 2b, c and Table 1. The electrode membrane layer consists of four layers, the first layer is PVA-Enzyme, the second layer GA 2.9 %, third layer PPy + H_2SO_4 or PPy + Sulfonic Acid, fourth layer PVC-KTpClPB-o-NPOE 61 %. Selected o-NPOE 61 % from the UV–vis analysis of Fig. 1. Compared to Fig. 2b, c and Table 1, the XRD diffraction spectrum pattern analysis showed a very large decrease in the amorphous spectrum pattern followed by an increase in the crystal spectral pattern (see Fig. 3).

* Corresponding author.
E-mail address: abdhakims@unimed.ac.id (S. Abd Hakim).

https://doi.org/10.1016/j.mset.2022.11.010
2589-2991/

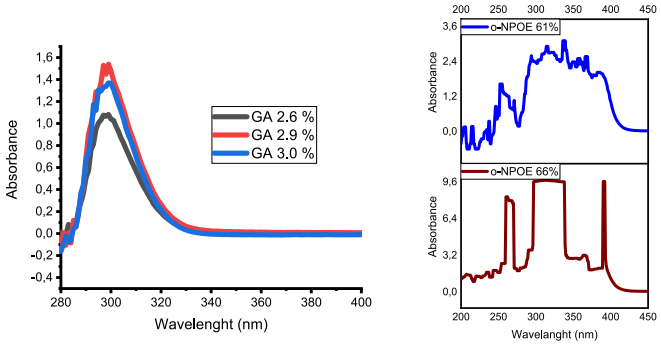

Fig. 1. UV–vis analysis of solutions (a) GA 2.6%, 2.9% and 3.0%, (b) PVC-KTpClPB-o-NPOE 61%, 66%.

This indicator electrode sample was selected to select the best electrode according to the layer modification which had analyzed the absorbance spectrum pattern of the PVA-enzyme immobilized layer; layer two GA crosslinks; PPy conduction polymer triple layer; and a layer of four o-NPOE plasticizers on PVC-KTpClPB [3]. After XRD analysis of samples EI5-1, EI5-3, EI4-1, EI4-3, the best samples were EI5-1 and EI4-1. Both samples were analyzed by FTIR, cell response potentiometer and linear curve analysis determining sensitivity, detection range, detection limit and R^2.

2. Methods

The method in this study is the biosensor potentiometric method [4–6] immobilization technique [7] urease enzyme which analytes urea, using potentimetric cells to determine the feasibility of urea sensors based on (1) response time of samples EI_5-1 and EI_4-1, (2) through linear curve analysis. Materials consist of 1.0 mm diameter tungsten 267 562 99.99 %, PVA [–CH_2CHOH-]n, enzyme EC 3.5.1.5 (Urease) U4002, Glutaraldehyde (GA), PPy, H_2SO_4, Sulphonic acid, PVC (CH_2CHCl) n, potassium tetrakis 4-chlorophenyl borate $(ClC_6H_4)_4BK$, tetrahydrofuran C_4H_8O, o-NPOE, KCl. Potentiometer (Keithley 199 DMM, USA), tungsten indicator electrode (W), Ag/AgCl MF-2052 rE-5B reference electrode in a microcomputer assembled electrochemical cell (ADI Powerlab instruments, Australia), magnetic stirrer and flow injection (FIA).

Table 1
Analysis of the EDX spectrum pattern of the indicator electrode (a) EI5-1, (b) EI5-3, (c) EI4-1, (d) EI4-3.

2Theta	EI_5-1	EI_5-3	EI_4-1	EI_4-3
44.48	140	220	166	236
44.5	164	228	210	216
44.54	204	176	224	172

3. Result and discussion

Fig. 1, shows the analysis of the indicator electrode with UV–vis [8–11] on GA solution [2] and o-NPOE solution in PVC-KTpClPB (PVC-KTpClPB-o-NPOE) [1,16–18]. The absorbance spectrum pattern with respect to the wavenumber of both shows a widening of the absorbance spectrum pattern for both GA and PVC-KTpClPB-o-NPOE. Analysis of Fig. 1a and 1b selected the best 2.9 % GA and PVC-KTpClPB-o-NPOE (o-NPOE 61 %). on the basis of coated indicator electrodes for the second and fourth layers.

Fig. 2, shows the analysis of the XRD diffraction spectrum pattern [18] for the indicator electrodes (a) EI_3-1-4 61 %, EI_3-1-4 66 %, EI_3-3-4 61 % and EI_3-3-4 66 %, (b) EI_5-1, EI_5-3, (c) EI_4-1, EI_4-3. In Fig. 2a the XRD diffraction spectrum pattern from EI_3-1-4 61 %, EI_3-1-4 66 %, EI_3-3-4 61 %, amorphous and crystalline spectrum patterns are formed with low intensity. In contrast to Fig. 2b EI_5-1 and EI_5-3, 2c EI_4-1 and EI_4-3 [19], a low amorphous spectrum pattern and high intensity crystals are formed. So it is clear that the pattern of the indicator electrode layers EI_5-1, EI_5-3 and EI_4-1, EI_4-3, varies in the number of drops of urease enzyme, one drop and three drops, respectively. The peak height of energy intensity with respect to the diffraction angle of 2theta can be seen in Table 1 (a) EI_5-1 high intensity 204 (a.u) at a diffraction angle of 44.54 degrees, (b) EI_5-3 high intensity 228 (a.u) at a diffraction angle of 44.5 degrees, (c) EI_4-1 high intensity 224 (a.u) at a diffrac-

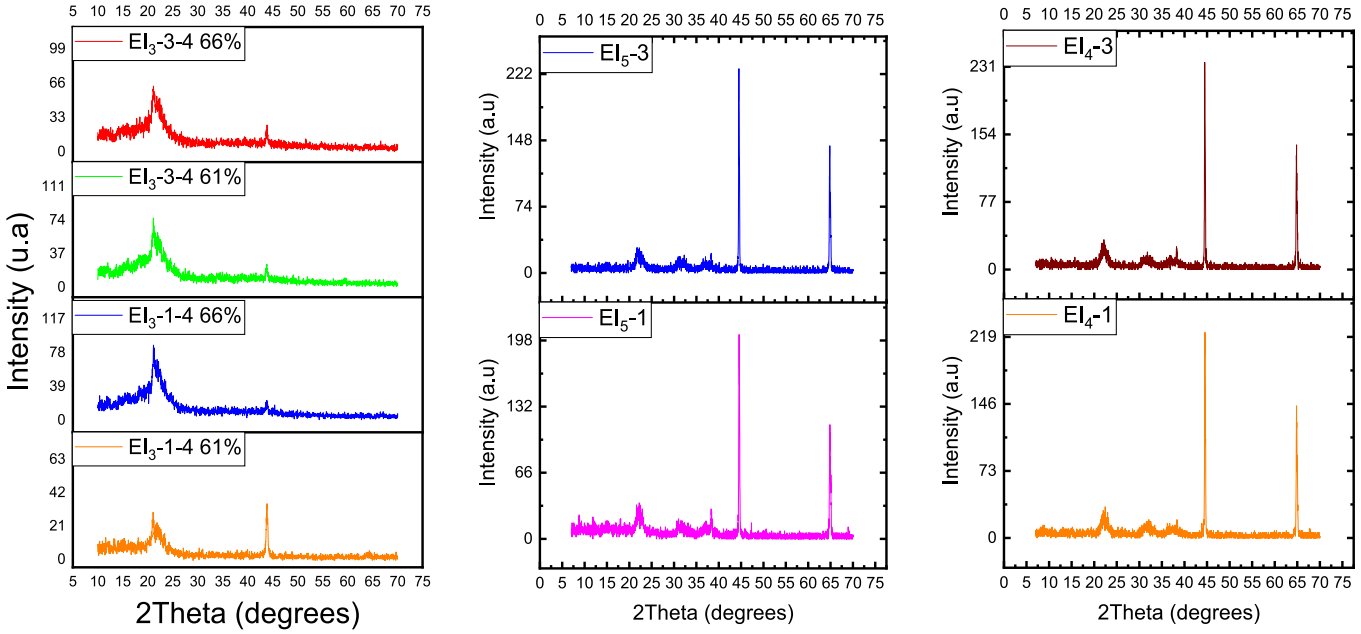

Fig. 2. Analysis of the XRD diffraction spectrum pattern of the indicator electrode (a) EI_3-1–4 61%, EI_3-1–4 66%, EI_3-3–4 61% and EI_3-3–4 66%, (b) EI5-1 and EI_5-3, (c) EI_4-1and EI_4-3.

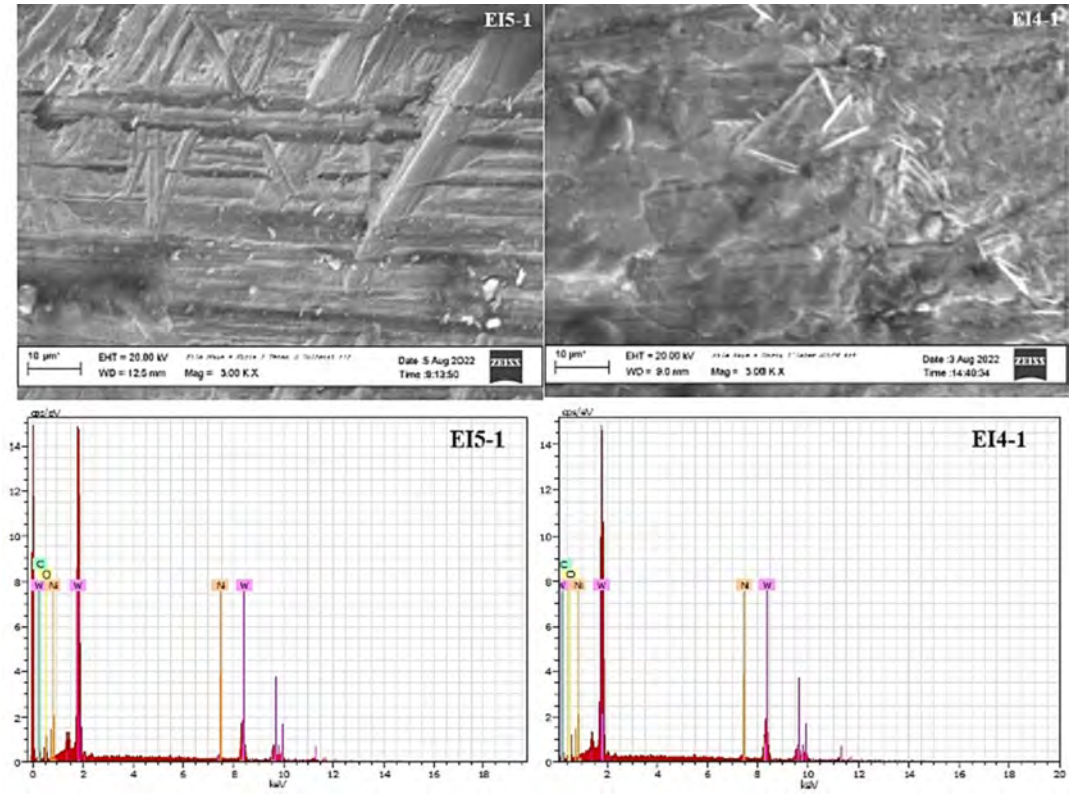

Fig. 3. SEM morphology and Spectrum pattern of intensity to EDX energy from indicator electrode (a) EI_5-1, (b) EI_4-1.

Table 2
Weight percentage of indicator electrodes from the EDX spectrum pattern of samples EI_5-1 and EI_4-1.

Indicator Electrodes	Material	unn. C [wt.%]	norm. C [wt.%]	Atom. C [at.%]	Error (1 Sigma) [wt.%]
EI_5-1	W 74 L-series	69.07	76.86	29.23	2.28
EI_4-1	W 74 L-series	81.95	83.86	32.85	2.65

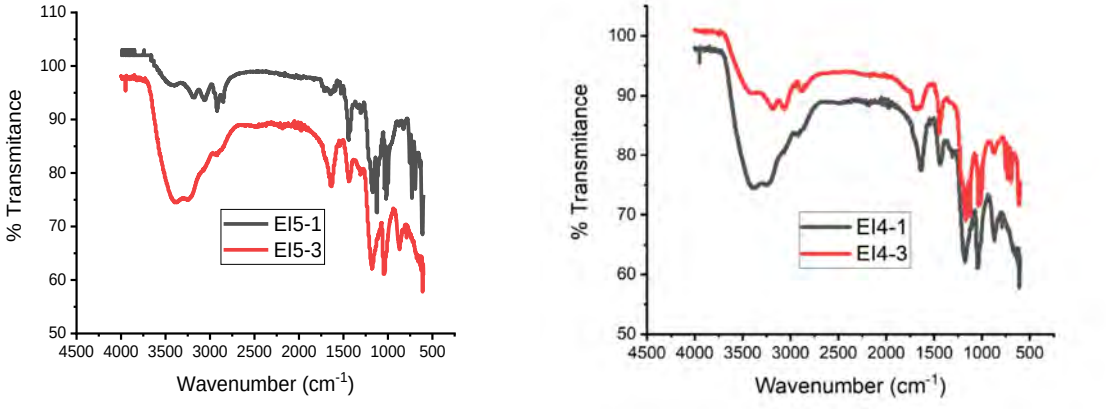

Fig. 4. The pattern of the transmittance spectrum against the wavenumber of the indicator electrodes (a) EI_5-1, EI_5-3, (b) EI_4-1, EI_4-3.

tion angle of 44.54 degrees, (d) EI_4-3 high intensity 236 (a.u) at a diffraction angle of 44.48 degrees.

Researchers are still continuing the analysis with SEM-EDX and FTIR [20] for clear assurance of the material used in the indicator electrodes (a) EI_5-1, (b) EI_5-3, (c) EI_4-1, (d) EI_4-3 as one sample best.

SEM morphology analysis with 3 Kx magnification at a voltage of 10 m 20 Kv resulted in a difference in energy intensity of 13.5 cps/keV 1 M sample EI_5-1 and energy intensity 14.7 cps/keV 8 M sample EI_4-1. Based on Table 1, it was obtained that the intensity of XRD analysis increased, Table 2 obtained that the data discrep-

Table 3
Table of transmittance ranges for sample wave numbers (a) EI4-1, (b) EI5-1.

Wavenumber (cm^{-1})	Transmittance (%)			
	EI_4-1	EI_4-3	EI_5-1	EI_5-3
600	60.8895	75.5583	75.9339	48.5782
4000	97.9351	100.9955	102.5625	100.8259

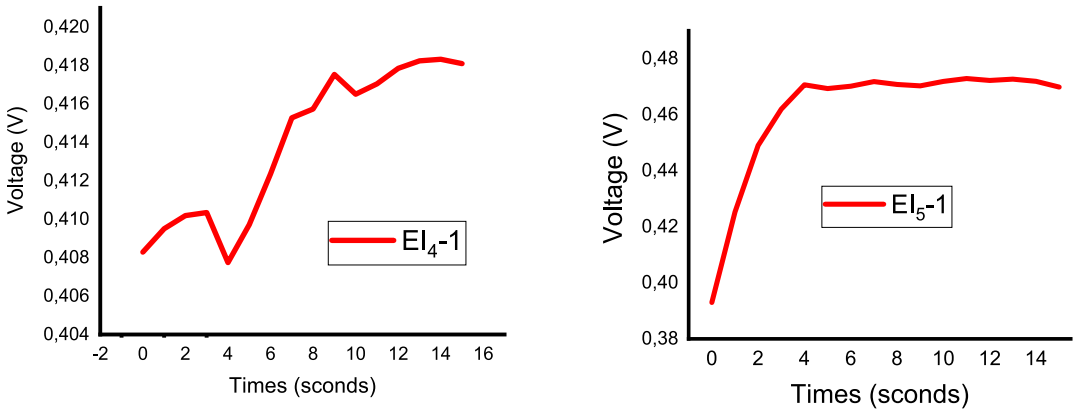

Fig. 5. Response time (a) EI4-1, (b) EI5-1.

Table 4
Linear curve of indicator electrodes EI_4-1 and EI_5-1.

Indicator electrode membrane layer	Sensitivity mV/decade	Detection range (M)	Detection limit (M)	R-square (R^2) (%)
EI_4-1	43.79	10^{-3}–10^{-1}	10^{-3}	98.83
EI_5-1	41.56	10^{-4}–10^{-1}	10^{-4}	97.51

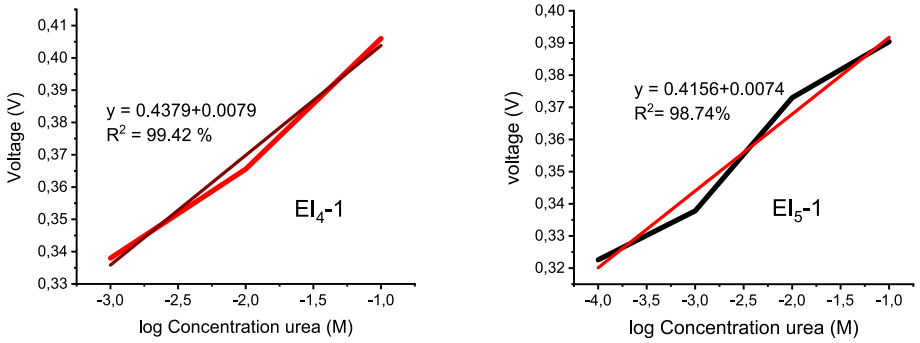

Fig. 6. Analisis kurva linear (1) EI_5-1, (b) EI_4-1.

ancy was greater in weight percent EI_4-1 than weight percent EI_5-1. While the FTIR analysis in Fig. 4 and Table 3 increases the transmittance for the indicator electrodes EI_5-1 and EI_5-3, on the contrary, the transmittance decreases for the indicator electrodes EI_4-1 and EI_4-3. XRD, FTIR and SEM-EDX analysis [6,21,22] then the best samples are EI_5-1 and EI_4-1.

After selecting two samples of indicator electrodes EI_5-1 and EI_4-1, according to the biosensor poenstiometry method, a potentiometer cell was used to test the feasibility of the indicator electrode response time (Fig. 5). The best response time analysis [6] Fig. 5a and b were obtained on the EI_5-1 sample also supported by the data in Table 4 that the EI_5-1 indicator electrode has a sensitivity of 41.56 mV/decade, a detection range of 10^{-4}–10^{-1} M, detection limit is 10^{-4} M and R^2 = 97.51 % [5,23]. The detection range of EI_5-1 is greater than that of EI_4-1, the detection range is 10^{-3}–10^{-1} M, the detection limit is 10^{-3} M, while R2 = 98.83 % [13,25,26].

In electrochemical detection, the signal associated with the interaction of the analyte is measured through the electrode. Measurements can be made by (a) connecting current and voltage, namely voltammetric and conductor metric biosensors; (b) current or voltage with respect to time, i.e., amperometric or potentiometric; (c) the imaginary versus the real part of the impedance, i.e., impedometric; (d) drain current versus line voltage in a FET biosensor [6], agreement with previously reported analyzes (i.e., FTIR, XRD, and SEM) [22] and confirming interactions with added organic modifiers (see Fig. 6).

The procedure of this study followed (a) Analysis of transmittance, edx, xrd [27], edx, xrd, linear curve, sensitivity and detection range [28], transmittance, concentration, sensitivity [29–31]; (b)

The biosensor system [20], namely (1) selectivity, (2) sensitivity, (3) linearity response, namely the concentration range of the target analyte to be measured, (4) reproducibility of signal response, samples having a different concentration. the same analyzed several times should give the same response, (5) fast response time and recovery time for reusability of the biosensor system, (6) stability and operating life; (c) The [7] immobilization technique was developed based on three important mechanisms, namely (1) physical adsorption, (2) covalent immobilization, (3) streptavidin–biotin immobilization. Achieving high sensitivity and selectivity requires minimization of nonspecific adsorption and stability.

4. Conclusion

As a conclusion from XRD, SEM-EDX and FTIR analysis, response time and linear curve analysis, the best sample is the EI_5-1 indicator electrode with four layer modifications, namely PVA-Enzyme/GA-2.9 %/PPy + Sulfonic Acid/PVC-KTpClPB-o-NPOE.

Acknowledgement

I would like to thank Medan State University for obtaining Applied Research in 2022, as well as data analysis collaboration with the Universitas Sumatera Utara.

References

[1] D. Vlascici, E.F. Cosma, I. Popa, V. Chiriac, M.G. Agusti, A novel sensor for monitoring of iron(III) ions based on porphyrins, Sensors 12 (2012) 8193–8203.
[2] J.L. Aparicio-Collado, J.J. Novoa, J. Molina-Mateo, C. Torregrosa-Cabanilles, Á. Serrano-Aroca, R.S. Serra, Novel semi-interpenetrated polymer networks of poly(3-hydroxybutyrate-co-3-hydroxyvalerate)/poly (vinyl alcohol) with incorporated conductive polypyrrole nanoparticles, Polymers 13 (2021) 57.
[3] E.H. El-Naby, Potentiometric Signal Transduction for Selective Determination of 1-(3-Chlorophenyl)piperazine "Legal Ecstasy" Through Biomimetic Interaction Mechanism, *Chemosensors* 7 (3) (2019), https://doi.org/10.3390/chemosensors7030046.
[4] M.S. Thakur, K.V. Ragavan, Biosensors in food processing, J Food Sci Technol 50 (4) (2013) 625–641.
[5] A.M. Al-Mohaimeed, New construction of functionalized CuO/Al2O3 nanocomposite-based polymeric sensor for potentiometric estimation of naltrexone hydrochloride in commercial formulations, Polymers 2021 (13) (2021) 4459.
[6] L. Bertel, D.A. Miranda, J.M. García-Martín, Nanostructured titanium dioxide surfaces for electrochemical biosensing, Sensors 21 (2021) 6167.
[7] S.B. Nimse, K. Song, M.D. Sonawane, D.R. Sayyed, T. Kim, Immobilization techniques for microarray: challenges and applications, Sensors 14 (2014) 22208–22229.
[8] M. Rezayi, L.Y. Heng, A. Kassim, S. Ahmadzadeh, Y. Abdollahi, H. Hossein Jahangirian, Immobilization of ionophore and surface characterization studies of the titanium(III) Ion in a PVC-membrane sensor, Sensors 12 (2012) 8806–8814.
[9] Singh, A. N., Singh, S., Dubey, V.K., (2013), Immobilization of Procerain B, a Cysteine Endopeptidase, on Amberlite MB-150 Beads, June | Volume 8 | Issue 6 | e66000, PLOS ONE | www.plosone.org.
[10] Sharma, N. K., Ameta, R. K., and Singh, M., (2016), From Synthesis to Biological Impact of Pd (II) Complexes: Synthesis, Characterization, and Antimicrobial and Scavenging Activity, Hindawi Publishing Corporation, Biochemistry Research International, Volume 2016, Article ID 4359375, 8 pages.
[11] N.A. Alarfaj, M.F. El-Tohamy, New functionalized polymeric sensor based NiO/MgO nanocomposite for potentiometric determination of doxorubicin hydrochloride in commercial injections and human plasma, *Polymers* 12 (12) (2020), https://doi.org/10.3390/polym12123066.
[13] S. Huang, F. Luo, X. Lai, Novel potentiometric sensors of ion imprinted polymers for specific binding of yttrium (III), Asian J. Chem. 26 (20) (2014) 6787–6790. https://doi.org/10.14233/ajchem.2014.16795.
[16] Elbehery, N. H. A., Amr, A. E.-G. E., Kamel, A. H., Elsayed, E. A., & Hassan, S. S. M. (2019). Novel Potentiometric 2,6-Dichlorophenolindo- phenolate (DCPIP) Membrane-Based Sensors: Assessment of Their Input in the Determination of Total Phenolics and Ascorbic Acid in Beverages. In Sensors 19(9). https://doi.org/10.3390/s19092058.
[17] A. Amr, A.H. Kamel, A.A. Almehizia, A. Sayed, H. Abd-Rabboh, Solid-contact potentiometric sensors based on main-tailored bio-mimics for trace detection of harmine hallucinogen in urine specimens, Molecules (Basel, Switzerland) 26 (2) (2021) 324, https://doi.org/10.3390/molecules26020324.
[18] A.M. Shawky, M.F. El-Tohamy, Highly functionalized modified metal oxides polymeric sensors for potentiometric determination of letrozole in commercial oral tablets and biosamples, Polymers 13 (9) (2021) 1384, https://doi.org/10.3390/polym13091384.
[19] Hakim S, A., (2021), Characterization of PVA-Enzyme Coated Indicator Electrodes GA coated again with PVC-KTpClPB-o-NPOE UV-Vis analysis, variable signal analysis, sensor sensitivity and SEM-EDS, JPPIPA 7(Special Issue).
[20] S.S. Alharthi, A.M. Fallatah, H.M. Al-Saidi, Design and characterization of electrochemical sensor for the determination of mercury(II) ion in real samples based upon a new schiff base derivative as an ionophore, *Sensors* 21 (9) (2021), https://doi.org/10.3390/s21093020.
[21] A.M. Al-Mohaimeed, A.E. Gamal Mostafa, M.F. El-Tohamy, New construction of functionalized CuO/Al2O3 nanocomposite-based polymeric sensor for potentiometric estimation of naltrexone hydrochloride in commercial formulations, Polymers 13 (2021) 4459.
[22] Wei Chen, Ping Zhu, Yating Chen, Yage Liu, Liping Du and Chunsheng Wu, 2022. Iodine Immobilized UiO-66-NH2 Metal-Organic Framework as an Effective Antibacterial Additive for Poly(ε-caprolactone) *Polymers* 2022, *14*, 283.
[23] M.A. Rahman, P. Kumar, D.S. Park, Y.B. Shim, Electrochemical sensors based on organic conjugated polymers, Review, Sensors 8 (2008) 118–141.
[25] Z.H. Ibupoto, S.M.U.A. Shah, K. Khun, M. Willander, Electrochemical L-lactic acid sensor based on immobilized ZnO nanorods with lactate oxidase, Sensors 12 (2012) 2456–2466.
[26] S. Elhag, Z.H. Ibupoto, O. Nur, M. Willander, Incorporating ß-cyclodextrin with ZnO nanorods: A potentiometric strategy for selectivity and detection of dopamine, Sensors 14 (2014) 1654–1664.
[27] Bibi, Aamna; Li, Ying-Hsuan; Jia, Hsi-Wei; Kuo, Hsien-po; Sathishkumar, Nadaraj; et al. 2022 Synthesis and characterization of biodegradable–electroactive polymer–Au nanocomposite materials for H2S sensing, Express Polymer Letters 16, 10 (2022) 1022–1037.
[28] M. Mashuni, H. Ritonga, M. Jahiding, B. Rubak, F.H. Hamid, Highly sensitive detection of carbaryl pesticides using potentiometric biosensor with nanocomposite Ag/r-graphene oxide/chitosan immobilized acetylcholinesterase enzyme, Chemosensors 10 (2022) 138, https://doi.org/10.3390/chemosensors10040138https://www.
[29] Er-Yuan Chuang; Ping-Yuan, Lin; Po-Feng, Wang; Tsung-Rong Kuo; Chen, Chih-Hwa; et al. 2021. Label-Free, Smartphone-Based, and Sensitive Nano-Structural Liquid Crystal Aligned by Ceramic Silicon Compound–Constructed DMOAP-Based Biosensor for the Detection of Urine Albumin, International Journal of Nanomedicine 2021:16 763–773
[30] Hui-Tzung Luh; Yi-Wei, Chung; Po-Yi, Cho; Yu-Cheng, Hsiao. 2022. Label-Free Cholesteric Liquid Crystal Biosensing Chips for Heme Oxygenase-1 Detection within Cerebrospinal Fluid as an Effective Outcome Indicator for Spontaneous Subarachnoid Hemorrhage, Biosensors, 12, 204. https://doi.org/10.3390/bios12040204.
[31] Sriwichai, Saengrawee; Phanichphant, Sukon 2022. Fabrication and characterization of electrospun poly(3-aminobenzylamine)/functionalized multi-walled carbon nanotubes composite film for electrochemical glucose biosensor, Express Polymer Letters 16, No.4 (2022) 439–450.

[12] Ulianas, A., Heng, L.Y., and Ahmad, M., (2011), A Biosensor for Urea from Succinimide-Modified Acrylic Microspheres Based on Reflectance Transduction, Article, Sensors 2011, 11, 8323-8338.

[14] M. Mir, R. Lugo, I.B. Tahirbegi, J. Samitier, Miniaturizable ion-selective arrays based on highly stable polymer membranes for biomedical applications, *Sensors* 14 (7) (2014), https://doi.org/10.3390/s140711844.
[15] H. Kaur, M. Chhibber, S.K. Mittal, Acyclic arylamine-based ionophores as potentiometric sensors for Zn2+ and Ni2+ ions, In *C.* 3 (4) (2017), https://doi.org/10.3390/c3040034.
[24] S.A. Hakim, T. Sembiring, K. Tarigan, K. Sebayang, M. Situmorang, N.M. Noer, Characterization of membrane PVA-enzyme coated PVC-KTpClPB as urea sensor with potentiometric method, Rasayan J. Chem. 12 (2019) 780–786. https://doi.org/10.31788/RJC.2019.1225143.